Cellulose (2024) 31:2475–2491
https://doi.org/10.1007/s10570-024-05758-3

ORIGINAL RESEARCH

Chlorophyllin as a photosensitizer in photodynamic antimicrobial materials

Chenyu Jiang · Frank Scholle · Fangyu Jin · Qufu Wei · Qingqing Wang · Reza A. Ghiladi

Received: 22 May 2023 / Accepted: 15 January 2024 / Published online: 8 February 2024

Abstract Self-disinfecting materials that are both safe and scalable for production are increasingly in demand, particularly in healthcare settings where they can be used to combat hospital-acquired infections (HAIs). Here, we employed the natural food colorant chlorophyllin (E140ii) as a photosensitizer to prepare photodynamic antimicrobial materials through both chemical conjugation and electrospinning, resulting in chlorophyllin-grafted cotton fabric (Chl-fabric) and chlorophyllin-embedded polyacrylonitrile nanofibers (Chl-NF), respectively. The materials were characterized by a number of physical methods, as was their ability to generate singlet oxygen upon visible light illumination. The best results with Chl-fabric yielded 99.998% inactivation of vancomycin-resistant *E. faecium* and 99.994% of methicillin-resistant *S. aureus* after 60 min visible light illumination (400–700 nm, 80 ± 5 mW/cm^2), whereas Chl-NF inactivated both bacteria by 99.9999%. Feline calicivirus was also photodynamically susceptible, with 99.8% inactivation by both materials. Gram-negative *Klebsiella pneumoniae* was not initially susceptible to photodynamic inactivation by Chl-NF, however addition of the photothermal agent MoS_2 fully inactivated (99.9999%) this pathogen under NIR illumination, indicative of synergistic photothermal and photodynamic activities. These findings suggest that chlorophyllin can be used in photodynamic antimicrobial materials against drug-resistant Gram-positive bacteria, and that its efficacy can be synergistically amplified in the presence of a photothermal agent against Gram-negative pathogens.

Supplementary Information The online version contains supplementary material available at https://doi.org/10.1007/s10570-024-05758-3.

C. Jiang (✉)
School of Optical and Electrical Information, Suzhou City University & Suzhou Key Laboratory of Biophotonics, Suzhou 215104, Jiangsu Province, China
e-mail: cjiang@szcu.edu.cn

F. Scholle
Department of Biological Sciences, North Carolina State University, Raleigh, NC 27695, USA

F. Scholle · R. A. Ghiladi
Center for Advanced Virus Experimentation, North Carolina State University, Raleigh, NC 27695, USA

F. Jin · Q. Wei · Q. Wang (✉)
Key Laboratory of Eco-Textiles, Ministry of Education, Jiangnan University, Wuxi 214122, Jiangsu Province, China
e-mail: qqwang@jiangnan.edu.cn

R. A. Ghiladi (✉)
Department of Chemistry, North Carolina State University, Raleigh, NC 27695, USA
e-mail: Reza_Ghiladi@ncsu.edu

Graphical abstract

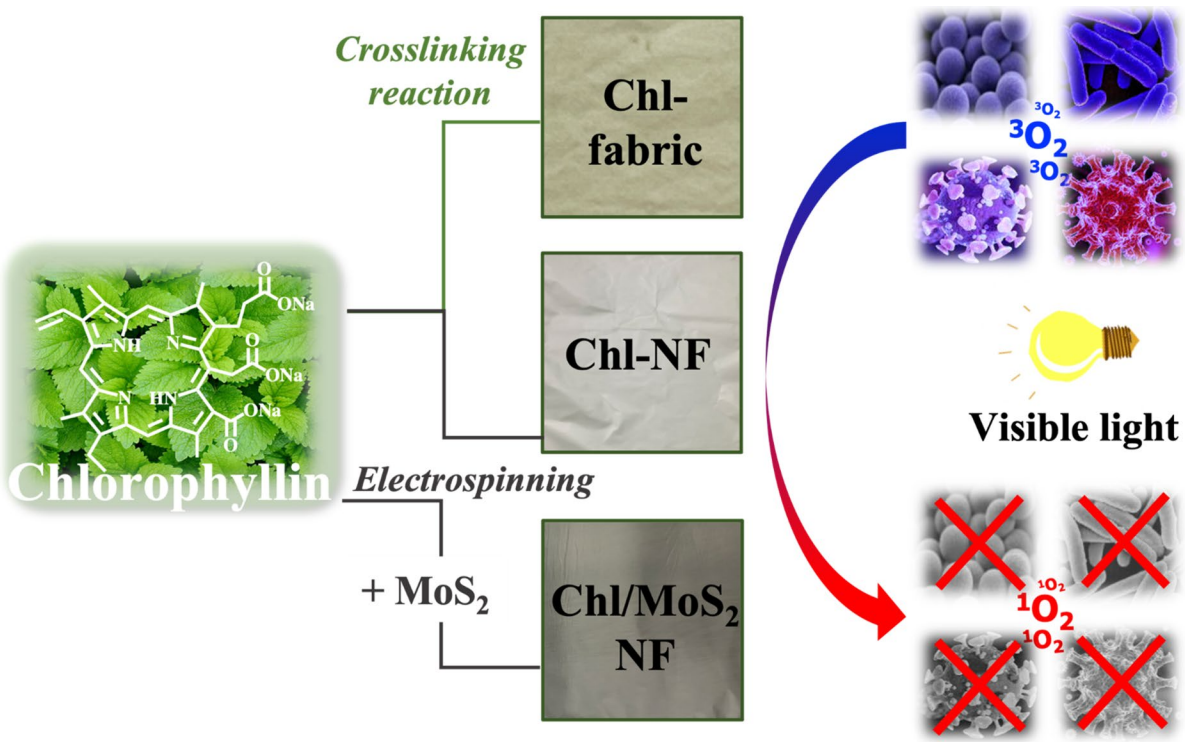

Keywords Antimicrobial · Chlorophyllin · Photodynamic inactivation · Photothermal inactivation

Introduction

Pathogen survival on high touch surfaces significantly contributes to the risk of transmission via fomites (Neely and Maley 2000). One such example of this risk are hospital-acquired infections (HAIs), where in just the United States alone, pathogen surface transmission results in 1 in 25 hospital patients being diagnosed with at least one infection related to hospital care, which annually causes nearly 1.7 million infections, ~ 100,000 deaths, and at a cost of $45 billion (Scott 2009). Not limited to bacterial infections, viruses can also be spread via fomites: to illustrate this point, the SARS-CoV-2 virus can remain stable on several surfaces for long periods of time (up to 2–3 days on stainless steel and unspecified plastic) (van Doremalen et al. 2020), and even upwards of 7 days on surgical masks (Chin et al. 2020). Regardless of the pathogen (bacteria, viruses, or even fungi), antimicrobial materials are increasingly in demand, particularly when it comes to self-disinfecting personal protective equipment (SD-PPE) commonly used in healthcare settings. Many strategies have been explored as the underlying antimicrobial mechanisms in SD-PPE, including embedding different bactericidal agents like antibiotics (Peila et al. 2013), quaternary ammonium salts (Zhang and Oyanedel-Craver 2013), and metal nanoparticles (Bober et al. 2014) into materials commonly used in PPE. While each of these has shown a measure of success, a number of limitations to these strategies remain, including their high-cost, poor efficacy against drug-resistant pathogens (Peddinti et al. 2018), inducing drug-resistance itself

(Maldonado-Carmona et al. 2020), environmental toxicity and/or unacceptable side effects, and the inability for them to be easily integrated into current PPE manufacturing lines (Stensberg et al. 2011).

Antimicrobial photodynamic inactivation (aPDI) has been explored as a possible strategy to overcome several of the aforementioned limitations in the design of SD-PPE. The underlying basis for aPDI is the generation of reactive oxygen species (ROS), including hydroxyl radicals (OH·), superoxide ($O_2^{\cdot -}$) and singlet oxygen ($^1O_2$), thus creating a highly oxidizing environment that is localized directly to the material surface. As microbicidal agents, the ROS produced through a photodynamic mode of action lead to the non-specific and irreversible damage to bacterial cell membranes or viral components, thus resulting in pathogen inactivation via necrosis or oxidative damage (Abrahamse and Hamblin 2016). Photodynamic inactivation is considered environmentally-friendly, as it relies upon a nontoxic photosensitizer, visible light, and molecular oxygen to generate the ROS. A number of different photosensitizers have been incorporated into aPDI-based materials, including rose Bengal (Alexandrino et al. 2019), toluidine blue-O (Decraene et al. 2006), methylene blue (Ghareeb et al. 2021), BODIPY dyes (Stoll et al. 2019), and tetrapyrroles (porphyrins (Carpenter et al. 2015), chlorins (Pucelik et al. 2020), and phthalocyanines (Anaya-Plaza et al. 2017)). Although the biosafety of these photosensitizers has been demonstrated in the dark, increased concerns over material safety persist, particularly when microbicidal photosensitizing agents are used as additives.

As a semi-synthetic derivative of the natural green pigment chlorophyll (Viera et al. 2019), the photosensitizer chlorophyllin is generally recognized as safe, and has been approved as a food colorant or a food supplement (E141ii) in Europe, the United States, and Brazil (Tumolo and Lanfer-Marquez 2012; Viera et al. 2019). More importantly, as suggested by the US Food and Drug Administration (FDA), chlorophyllin can be safely ingested up to 300 mg per day (21 CFR 357.850). Relevant to our work here, a recent report has shown that 2.5 μM (1.8 mg/L) E141ii solution was able to inactivate 99.9999% methicillin-sensitive *S. aureus* (ATCC 25923) after 60 min visible-light illumination (625 nm, 30 J/cm^2) (Caires et al. 2020). However, to our best of our knowledge, studies incorporating chlorophyllin E141ii into photodynamic antimicrobial materials are limited, and questions remain regarding the design, scope, and efficacy of materials employing chlorophyllin as a photosensitizer, particularly when used in combination with other photosensitizers or photothermal agents.

To address these questions, we employed two different methods, chemical conjugation via triazine-coupling and high voltage electrospinning, to prepare photodynamic materials with chlorophyllin as the photosensitizer. Many methods have been successfully developed to prepare photosensitizer conjugated cellulose materials (Fadavi et al. 2019; Hettegger et al. 2015). The coupling agent 2,4,6-trichloro-1,3,5-triazine, also known as cyanuric chloride, has been devoted to covalently attach a number of photosensitizers to various cellulose scaffolds, with the reported advantages of (1) ambient reaction conditions, (2) no metal-based catalyst was needed, and (3) no chromatography was needed for purification (Alvarado et al. 2019; Wang et al. 2020). Similarly, electrospinning has been successfully adopted to embed various photosensitizers into polymers such as nylon and polyacrylonitrile (Stanley et al. 2016; Stoll et al. 2019). The electrospun fibers possess a number of characteristics important for aPDI, including a high surface area that allows for increased photosensitizer and pathogen interaction. Given the facile nature of both these methods to produce photodynamic materials, here we present the synthesis, characterization, and aPDI studies of chlorophyllin-grafted cotton fabric (Chl-fabric) and chlorophyllin-embedded polyacrylonitrile nanofibers (Chl-NF). The materials were characterized by both physical (SEM, ICP-OES, TGA) and colorimetric (*K/S*, *CIELab* values) methods, and their ability to generate singlet oxygen was also evaluated. Photodynamic inactivation studies were performed with both materials using Gram-positive/-negative bacteria as well as a non-enveloped virus under different illumination conditions, and the photostability of the Chl-fabric was also investigated. To explore if chlorophyllin was compatible with other photodynamic agents, we also incorporated molybdenum disulfide (MoS_2) as a photothermal agent into polyacrylonitrile via electrospinning, and compared the activity of the dual-agent chlorophyllin/MoS_2-nanofiber (Chl/MoS_2-NF) against its single-agent material counterparts, Chl-NF and MoS_2-NF. Based on our previous study (Shen et al. 2021), no mammalian cell cytotoxicity was observed for MoS_2 when loaded onto a cellulose membrane at the same concentration employed here.

The results demonstrate that chlorophyllin is a promising candidate for photodynamic antimicrobial materials from which SD-PPE can be produced without concerns for the biosafety of the photosensitizer.

Materials and methods

Materials

Chlorophyllin was purchased from Hubei Yunmei Technology Co. (Batch No. 20210408). Polyacrylonitrile powder (PAN: MW = 150,000, 99%) was purchased from Shaoxing Gimel Advanced Materials Technology Co., Ltd. Commercially available cotton yarns (80 S/2) with a plain weave (115 × 152) structure were woven by Changhong Textile Co. Molybdenum disulfide (MoS_2) ultrafine powder was purchased from Nanjing XFNANO Materials Tech Co. All other chemicals were of laboratory grade and used as received from commercial sources without further purification.

Preparation of chlorophyllin-grafted cotton fabric (Chl-fabric), chlorophyllin-embedded PAN nanofibers (Chl-NF), MoS_2-embedded PAN nanofibers (MoS_2-NF) and chlorophyllin/MoS_2 dual-embedded PAN composite nanofibers (Chl/MoS_2-NF)

Pristine cotton fabric was cut into 15 cm × 15 cm (~ 5 g) squares that were individually soaked in 0.5 M NaOH at 40 °C for 2 h and the fabric was then placed in 200 mL 5 mM cyanuric chloride tetrahydrofuran solution, and incubated for 12 h at 40 °C. After the reaction period, deionized water and tetrahydrofuran were used to wash out the unreacted cyanuric acid and other impurities. The activated fabric was then submerged in 200 mL 1.25 mM chlorophyllin aqueous solution at 40 °C for another 12 h. The conjugated fabric was first dried at 40 °C, and then washed with deionized water to remove any remaining free chlorophyllin. To ensure the absence of any unbound photosensitizer, the fabric was further submerged in deionized water (3 mL/cm^2 fabric) for 1 h and vortexed before the aqueous solution was transferred to a cuvette and its absorption spectrum recorded. When the spectrum of free chlorophyllin could no longer be observed within the detection limit of the spectrometer, the resultant Chl-fabric was then dried at 40 °C in an oven and stored in the dark until further use.

The electrospinning solution was prepared by first dissolving 1.5 g polyacrylonitrile (PAN) powder into 15 mL DMF solvent with stirring until no aggregation was observed, followed by the addition of either 0.0375 g chlorophyllin (at 2.5 wt% with respect to the mass of PAN), 0.15 g MoS_2 powder (at 10 wt% with respect to the mass of PAN) or both. The solution was further stirred for 12 h prior to electrospinning with the following parameters: needle-to-collector distance, 15 cm; voltage, 15 kV; solution feeding speed of the syringe pump, 1 mL/h. The electrospun fiber was collected on aluminum foil. As described above for Chl-fabric, UV–visible spectroscopy was employed to ensure the absence of free chlorophyllin or MoS_2. The Chl-NF, MoS_2-NF, and Chl/MoS_2-NF materials were stored in the dark until further use.

Physical characterization

Inductively coupled plasma-optical emission spectroscopy (ICP-OES)

The amount of chlorophyllin in both Chl-fabric and Chl-NF were determined by ICP-OES (NC State University Environmental and Agricultural Testing Service). Adapted from a previously published protocol (Ghareeb et al. 2021), chlorophyllin was extracted from Chl-fabric via overnight soak in ultrapure nitric acid, and from Chl-NF via nanofiber dissolution in DMF solvent followed by ashing. The amount of chlorophyllin was calculated based on the detected copper impurity when compared to an authentic sample of chlorophyllin, and the calculation details are found in Table S1 and Table S2.

Photometry and colorimetric characteristics

The colorimetric characteristics [*CIE (L*, a*,* and *b*)* color space and color depth (*K/S*)] of the pristine cotton fabric, Chl-fabric, Chl-NF, MoS_2-NF and Chl/MoS_2-NF materials were evaluated using a Datacolor 650 spectrophotometer (USA) employing a D65 light source with an aperture of 9 mm. Each sample was folded into 2 layers to give a sufficient thickness to prevent show-through. The *K/S* values of the

fabrics were calculated by the Kubelka–Munk function (Eq. 1) as follows:

$$K/S = (1 - R)^2/2R \quad (1)$$

where K and S are the absorption and scattering coefficient of the fabrics, and R is the reflectance of the samples at λ_{max}. All spectra were normalized to the baseline absorption at 700 nm.

Scanning electron microscopy (SEM)

The surface morphologies of the pristine cotton fabric, Chl-fabric, Chl-NF and Chl/MoS_2-NF materials were visualized with a SU1510 (Hitachi, Ltd., Japan) scanning electron microscope with an accelerating voltage of 5.0 kV. Images were collected at 1000×, 5000× or 10,000× magnifications at room temperature. Prior to SEM imaging, the prepared samples were fixed on a metal plate by conductive resin and were sputtered with a thin layer of gold nanoparticles.

Thermal gravimetric analysis (TGA)

The thermal degradation behaviors of pristine cotton fabric, Chl-fabric, pure PAN nanofibers, Chl-NF and Chl/MoS_2-NF materials were studied under an inert nitrogen atmosphere using a thermogravimetric instrument (TGA, SDTA 851, Beijing). Each sample (~5 mg) was heated in a platinum pan sample holder from 30 to 790 °C at a rate of 10 °C/min.

Photothermal properties

To understand the photothermal characteristics of Chl-NF and Chl/MoS_2-NF compared to MoS_2-NF, the samples were illuminated with an IR lamp (100 W, 760 nm ≤ λ ≤ 5000 nm, 15 cm sample distance) for 20 min. An infrared thermal imager (FLIRC 7200, FLIR, USA) was utilized to simultaneously record the real-time temperature of the samples and obtain photothermal images every 5 min.

Singlet oxygen detection via photoluminescence

The Chl-fabric, Chl-NF, MoS_2-nanofiber and Chl/MoS_2-NF materials were cut into 3 cm × 3 cm squares and fixed to glass slides via double-sided tape. The photoluminescence spectra were measured on an Edinburgh fluorimeter (FS920) equipped with a near-IR photomultiplier tube using 400 nm excitation. Due to the weak nature of the $^1O_2$ phosphorescence emission band at 1278 nm, the excitation bandwidth was 5 nm, and the emission bandwidth was 15 nm. Emission intensities were baselined and integrated from 1250 and 1330 nm.

Antimicrobial photodynamic inactivation studies

Bacterial cell culture

Multi-drug resistant *A. baumannii* (MDRAB, ATCC-1605) was grown in LB-Miller broth, methicillin-resistant *S. aureus* (MRSA, ATCC-44) and methicillin-susceptible *S. aureus* (ATCC-6538) were grown in tryptic soy broth (TSB), *K. pneumoniae* (KP, ATCC- 2146) was grown in BD Difco Nutrient Broth #234000, and vancomycin-resistant *E. faecium* (VRE, ATCC-2320) was grown in BD Difco Bacto Brain Heart Infusion #237500. Bacterial strains were grown to an initial concentration of 1–5 × 10^8 CFU/mL and the concentration of the cultures was monitored by optical density measurements at 600 nm (OD_{600}) using a Thermo Electron Corporation Genesys 10 UV–VIS scanning spectrophotometer. Cultures were pelleted via centrifugation at 4150 rpm for 10 min, the supernatant was decanted, and the bacteria were resuspended in 5 mL of phosphate buffered saline (PBS; aqueous solution of 170 mM NaCl, 3.4 mM KCl, 10.0 mM Na_2HPO_4, 1.8 mM KH_2PO_4, pH ~ 7.2) containing 0.05% Tween-80 prior to the aPDI assay.

Light sources

A LumaCare USA model LC122 PDT non-coherent light source (PDT light) was employed for antimicrobial photodynamic inactivation studies. The lamp was equipped with an OSRAM 64653 HLX Xenophot bulb (250 W, 24 V), and employed a LUM V (400–700 nm band pass filter) fiber optic probe with a ~ 95 ± 3% average transmittance (T_{avg}). A commercially available white LED Light (10 W) and common hood light were also employed to simulate real-world illumination conditions. Fluence rates at different wavelengths of the three light sources were measured in units of mW/cm^2 with an Ophir Orion power

meter (Table S3). A xenon lamp (500 W) equipped with a long-pass filter ($\lambda \geq 420$ nm) placed at a vertical distance of 15 cm from the sample or assay was employed to both photobleach the Chl-fabrics and perform their corresponding aPDI assays against *S. aureus.*

Antibacterial photodynamic inactivation assays

Photodynamic inactivation studies were performed in sterile, flat-bottom 24-well plates (BD Falcon). Briefly, samples were cut into 1 cm × 1 cm squares, and individually placed into three adjacent wells of a 24-well plate. A 100 µL aliquot of bacterial suspension in PBS from Sect. "Bacterial cell culture" above was added to each of the three wells. The 24-well plate was then illuminated under the light source for a fixed illumination time as indicated in the figure legends. Another 24-well plate containing two samples was also prepared using the same procedure but was kept without illumination as the dark control. Following illumination, 0.9 mL sterile PBS was added to each well in both the illuminated and the dark control plates, and the plates were manually stirred with a pipet to resuspend the bacteria. Each sample well was then 1:10 serially diluted (40 µL in 0.36 mL aliquots of PBS) six times, and 10 µL from each diluted well were separately plated in columns on gridded six column square plates (LB- media-agar MDRAB, TSB-agar for MRSA and *S. aureus,* BD Difco Nutrient Broth #234000-agar for *K. pneumoniae*, and BD Difco Bacto Brain Heart Infusion #237500-agar for vancomycin-resistant *E. faecium*), followed by overnight dark incubation at 37 °C. Two material-free dark control samples were prepared by aliquotting 100 µL bacterial PBS solution into 0.9 mL sterile PBS, and following the same serial dilution and plating process. The number of visible colonies on the agar plates was determined by colony counting, and the survival rate was determined by the average ratio of CFU/mL of the illuminated or dark plates versus the average ratio of the corresponding material-free controls. The detection limit was 6 log units of inactivation when starting with a concentration of 10^8 CFU/mL. Survivability values limited to $\geq 0.0001\%$ were recorded, with this value representing the detection limit. Statistical significance was assessed using an unpaired Student's two-tailed t-test.

Photostability of chlorophyllin conjugated cotton fabric

Chl-fabric was cut into 3 cm × 3 cm samples that were then illuminated at a vertical distance of 15 cm from a xenon lamp (500 W) equipped with a long-pass filter ($\lambda \geq 420$ nm) for either 2, 4, 6 or 8 h, after which they were stored in the dark until use. The above aPDI assays and controls were adopted to evaluate the antibacterial efficacy of the photobleached Chl-fabrics against *S. aureus*. The *K/S* values of the photobleached Chl-fabrics were also recorded as described above.

Antiviral photodynamic inactivation studies

Feline calicivirus was grown to a titer of 10^9 $TCID_{50}$/mL on the Crandall-Reese Feline Kidney (CRFK) cell line in cell growth media (DMEM, 1% antibiotics, 10% fetal bovine serum, FBS) at 35 °C. Three cut pieces (6 mm diameter) of a material sample were fitted into the well-bottoms of a 96-well plate, and 25 µL of virus suspension (free of the host CRFK cells) were added into each sample-containing well for the illuminated studies, and into 3 empty wells separately for the material-free illuminated controls. The prepared 96-well plate was illuminated under different light sources for defined times as indicated in the figure legends. Another 96-well plate was identically prepared but was wrapped by aluminum foil and left for the same defined illumination time, but without illumination, for the dark controls and the material-free dark controls. After illumination, 75 µL infection media (DMEM 1% antibiotics, 1% FBS, 1% HEPES buffer) were added to the wells in both plates, and the virus was eluted by triturating several times, followed by rapid transfer to new wells. Virus suspensions were immediately diluted serially ten-fold, and 50 µL of four replicates of each dilution were used to infect CRFK cells seeded the previous day at a density of 10^4 cells per well in a $TCID_{50}$ assay protocol. The plates were incubated at 35 °C with 5% CO_2. After 72 h, the cytopathic effect was monitored by visual inspection, and the resulting $\log_{10}$ $TCID_{50}$/mL values (minimum detection limit/MDL of 2.8 $\log_{10}$ $TCID_{50}$/mL) were calculated according to the Spearman-Kaerber method.

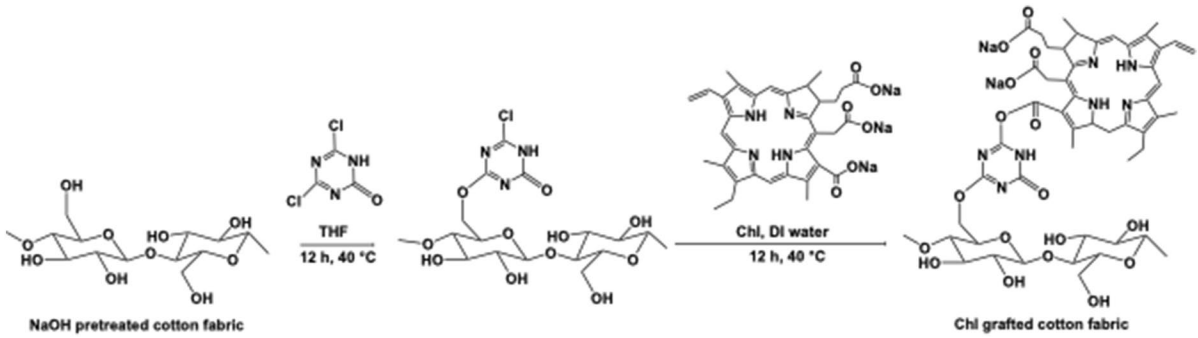

Scheme 1 Synthesis of chlorophyllin-conjugated cotton fabric (Chl-fabric) via 2,4,6-trichloro-1,3,5-triazine coupling, and the corresponding photographic images of pristine cotton fabric (left) and Chl-fabric (right)

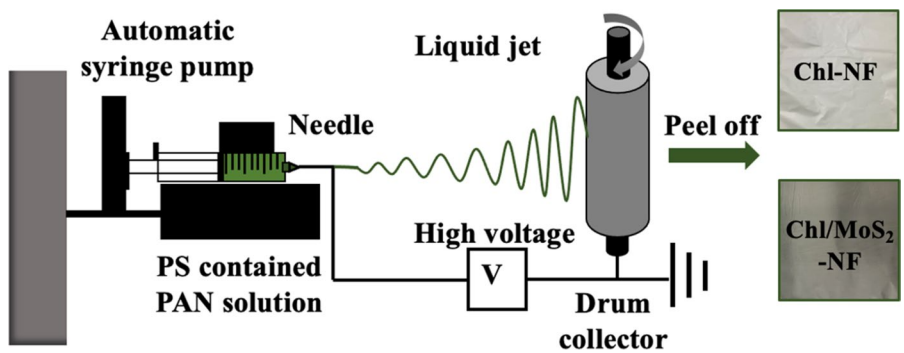

Scheme 2 Electrospinning schematic and photographic image of chlorophyllin-embedded polyacrylonitrile nanofibers (Chl-NF) and chlorophyllin/MoS_2 dual-embedded nanofibers (Chl/MoS_2-NF)

Results and discussion

Material characterization

Material preparation and chlorophyllin loading

Chl-fabric was prepared by the conjugation of chlorophyllin to cotton fabric via 2,4,6-trichloro-1,3,5-triazine (TCT) coupling (Scheme 1). The pristine cotton fabric was initially pretreated by soaking in NaOH for 2 h at 40 °C and then treated with TCT, followed by reaction with the chlorophyllin photosensitizer to yield the desired chlorophyllin conjugated cotton fabric (Chl-fabric). While some inter-strand crosslinking has been shown in previous studies (Alvarado et al. 2019) to occur upon reaction of cellulose with TCT, sufficient non-crosslinked cellulose-TCT remains available for subsequent reaction with the photosensitizer. Chl-nanofiber (Chl-NF), MoS_2-nanofiber (MoS_2-NF) and Chl/MoS_2-nanofiber (Chl/MoS_2-NF) materials were prepared by simply mixing predissolved polyacrylonitrile in DMF solution with either chlorophyllin, MoS_2 or both, followed by electrospinning (Scheme 2). The physical appearance of both Chl-fabric and Chl-NF presented an obvious color change to green corresponding to the inherent color of chlorophyllin, which visually indicated the successful loading of the photosensitizer into both materials. Compared to Chl-NF, Chl/MoS_2-NF presented a color combination of green and grey coming from both chlorophyllin and MoS_2, respectively. The quantitative analysis of loaded chlorophyllin was determined by ICP-OES based on the presence of trace copper in the commercial chlorophyllin sample, and was found to be 0.41 nmol Chl/mg cotton for Chl-fabric, and 5.19 nmol Chl/mg PAN for Chl-NF. Compared to other PS-cellulose materials produced via triazine-coupling, including hypocrellin-grafted bacterial cellulose (155 nmol PS/mg material) (Wang et al. 2020) and porphyrin-grafted cellulose paper (109 nmol PS/mg material) (Alvarado et al. 2019), the loading of chlorophyllin is significantly lower, and is likely due to the lower surface area of the cotton yarn fibers employed here as opposed to the nanofiber

dimensions of bacterial cellulose and nanofibrillated cellulose, respectively, used in those previous studies. In line with the low loading of chlorophyllin, the spectroscopic methods employed here were unable to conclusively demonstrate the presence of the covalent linkage via triazine-coupling (due to the low degree of substitution), however those aforementioned previous studies have demonstrated the cellulose-triazine-PS covalent linkage. While the chlorophyllin concentration was much higher in Chl-NF than Chl-fabric, it was still lower than other PS-embedded polyacrylonitrile-based electrospun materials, such as BODIPY$^{(+)}$-PAN (21.1 nmol PS/mg material) (Stoll et al. 2019) and Por$^{(+)}$-PAN (34.8 nmol PS/mg material) (Stanley et al. 2016). The negative charge of chlorophyllin may be relevant to its poorer retention in polyacrylonitrile as the polar nitrile group possess a high dipole moment (3.9 D (Wu et al. 2012)), with the nitrogen likely forming a stronger electrostatic interaction with positively-charged photosensitizers like BODIPY$^{(+)}$and Por$^{(+)}$-PAN compared to chlorophyllin. The effect of PS loading on the antimicrobial and antiviral activity of both Chl-fabric and Chl-NF will be discussed later.

Colorimetric analysis

The color space coordinates [light–dark *(L*)*, red-green (*a**), and yellow-blue (*b**) values] for pristine cotton fabric, Chl-fabric, Chl-NF, MoS_2-NF and Chl/MoS_2-NF are provided in Fig. 1 and Table 1. The pristine cotton fabric was off-white in appearance with a value of − 0.09 for a*. After the loading of chlorophyllin, the *a** value of Chl-fabric showed a decrease to − 2.27 compared to the pristine fabric, consistent with the visual color change of the fabric toward green as shown in Fig. 1A and Scheme 1. Compared to the Chl-fabric, Chl-NF has a greater negative *a** of − 3.73, which is consistent with the higher loading of chlorophyllin in the electrospun material as demonstrated by the ICP-OES results described above. The color depth (*K/S* values) was determined by light reflectance measurements, and the corresponding *K/S* curves are shown in Fig. 1B. It was noted that both Chl-fabric and Chl-NF exhibited two characteristic peaks ca 400 and 660 nm, which match well with the absorption features of chlorophyllin in aqueous solution (Figure S1), while pristine cotton fabric only exhibited a minor absorption below 450 nm. MoS_2-NF exhibited a broad peak around 600 nm, which is consistent with the absorption peak of MoS_2 and indicative of the successful loading of MoS_2 into the nanomaterial (Shen et al. 2021).

Table 1 *CIELab* values of pristine cotton fabric, Chl-fabric, Chl-NF, and Chl/MoS_2-NF

	L*	a*	b*
Pristine fabric	93.16	− 0.09	3.13
Chl-fabric	87.79	− 2.27	9.93
Chl-NF	87.19	− 3.72	12.79
Chl/MoS_2-NF	62.41	− 2.04	5.79

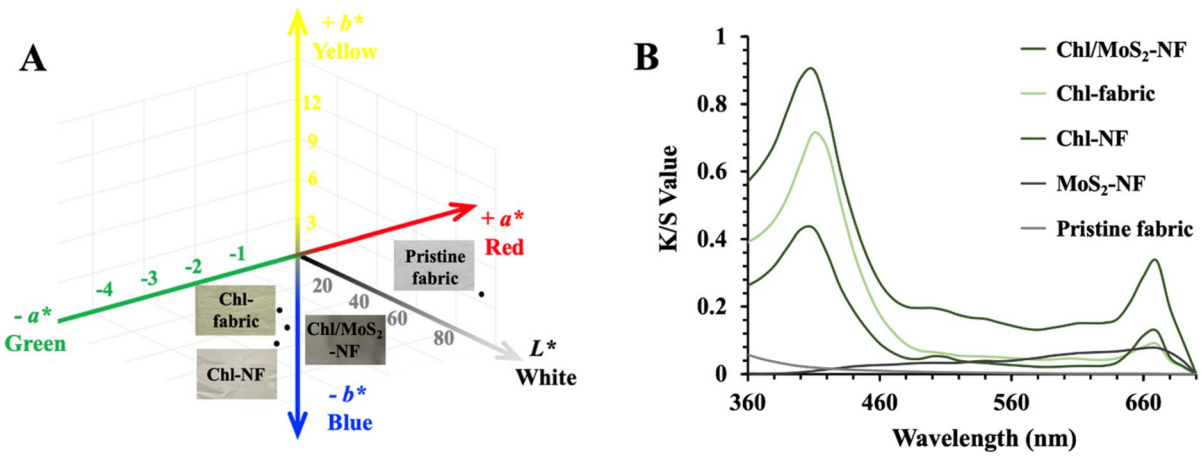

Fig. 1 **A** *CIELab* coordinates and **B** *K/S* curves for pristine cotton fabric, Chl-fabric, Chl-NF, MoS_2-NF and Chl/MoS_2-NF

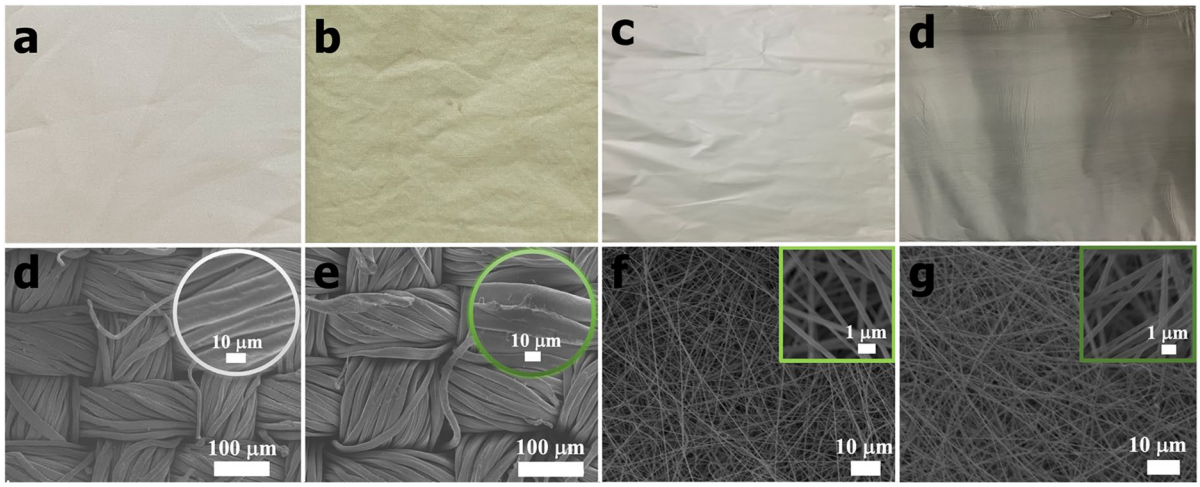

Fig. 2 Photographic (top) and SEM images (bottom) for **a**, **d** pristine cotton fabric, **b**, **e** Chl-fabric, **c**, **f** Chl-NF and **d**, **g** Chl/MoS_2-NF

Scanning electron microscopy (SEM)

The surface morphological features of pristine cotton fabric, Chl-fabric, Chl-NF, and Chl/MoS_2-NF were investigated by scanning electron microscopy (SEM) under different magnifications (Fig. 2). Continuous cotton fibers with typical convolutions and a kidney-shaped structure (Messiry et al. 2015) can be observed for both pristine cotton fabric and the Chl-fabric under × 100 magnification (Fig. 2d, e). Some crisscross patterns can be found on the surface of the cotton fiber under × 1000 magnification (Fig. 2e) owing to the non-structured orientation of cellulose and non-cellulosic materials from the primary walls (the secondary layer of cotton fibers), while only smooth grooves (Fig. 2d) corresponding to the wax layer on the cuticle were observed for pristine fabric (Klemm et al. 2005), indicative of a minor amount of surface damage to the cotton fiber during the coupling reaction. However, neither compact parallel structures corresponding to the highly ordered crystalline cellulose of the inner secondary wall, nor broken cotton fibers, were observed, which demonstrate that the surface damage was limited.

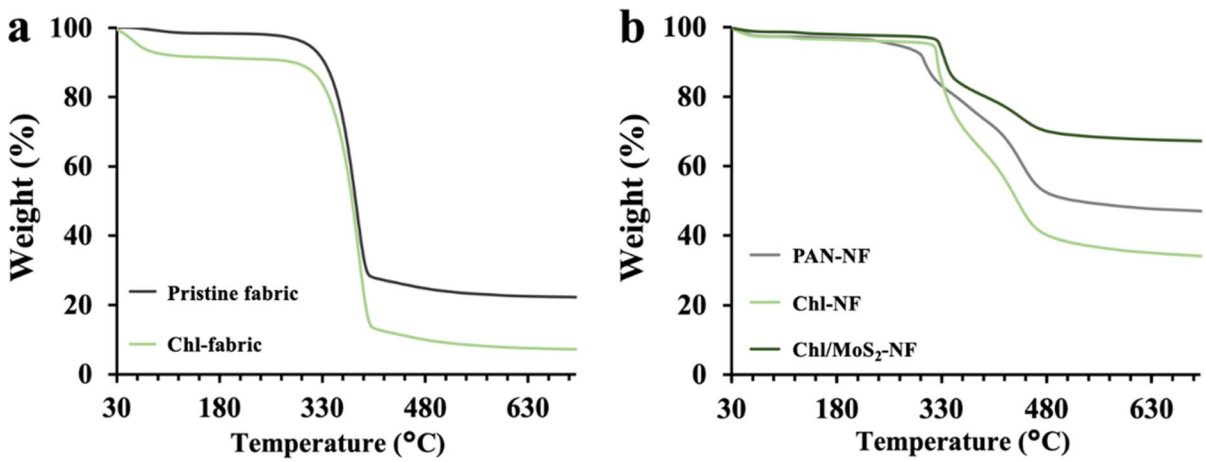

Fig. 3 Thermal gravimetric analysis of **A** pristine cotton fabric and Chl-fabric, and **B** pure PAN nanofibers, Chl-NF and Chl/MoS_2-NF

The nanofiber dimensions of the electrospun PAN in Chl-NF and Chl/MoS_2-NF were also confirmed by SEM. Under × 1000 magnification (Fig. 2f, g), continuous fibers with a nearly uniform diameter were observed, and their smooth surfaces match well with those observed for pure PAN nanofibers (Stoll et al. 2019), suggesting that neither chlorophyllin nor MoS_2 incorporation had an effect on the morphology or structure of the nanofibers.

Thermal gravimetric analysis (TGA)

The thermal decomposition profiles of pristine cotton fiber, pure PAN nanofibers, Chl-fabric, Chl-NF, and Chl/MoS_2-NF materials were investigated using thermal gravimetric analysis (Fig. 3). In the first stage up to 100 °C, a minor initial weight loss of around 1–5% were noted for all materials that was attributed to the evaporation of adsorbed moisture in the materials. Pristine cotton fabric and Chl-fabric exhibited a similar onset temperature of main stage loss at around 300 °C and 305 °C, respective (Fig. 3A). Interestingly, Chl-NF exhibited a significantly more stable thermal property than pure PAN nanofibers, with the onset temperature of main stage loss increasing from 270 to 320 °C (Fig. 3B). We surmise that this improved stabilization for Chl-NF was due to the presence of chlorophyllin, as the degradation of tetrapyrroles usually occurs above 390 °C (Norman et al. 2016). The fact that this chlorophyllin-dependent thermal stabilization was not observed for Chl-fabric (compared to pristine cotton) is likely due to the 13-fold lower loading of chlorophyllin in Chl-fabric vs. Chl-NF. Compared to Chl-NF, the addition of MoS_2 does not pose any negative effects on the photothermal stability with a similar onset temperature of Chl/MoS_2-NF around 320 °C. Overall, Chl-fabric, Chl-NF and Chl/MoS_2-NF were thermally stable to 300 °C, suggesting all the materials are sufficiently thermally robust for real-world applications as SD-PPE.

Thermal properties

The photothermal properties of the MoS_2-NF (M) and Chl/MoS_2-NF (CM) materials were evaluated using IR images captured in 5 min intervals under continuous illumination by an IR lamp (100 W, 760 nm ≤ λ ≤ 5000 nm, and 15 cm sample distance) using the Chl-NF (C) material as a reference (Fig. 4a). As illustrated in Fig. 4b, within the first 5 min of IR illumination, both MoS_2-NF and Chl/MoS_2-NF exhibited an increase in temperature to ~ 41 °C, while Chl-NF only reached ~ 36 °C. Over the entire 20 min illumination period, higher temperature increases were observed for both MoS_2-NF and Chl/MoS_2-NF (T_{final} = 52.9 and 55.0 °C, respectively) when compared with Chl-NF (T_{final} = 43.1 °C), indicating that MoS_2 was serving (as designed) as a photothermal sensitizer. Furthermore, the uniform temperatures observed across the samples indicated the even distribution of MoS_2 within the nanomaterials, whereas the similar thermal profiles of both MoS_2-NF and Chl/MoS_2-NF suggested that the presence of

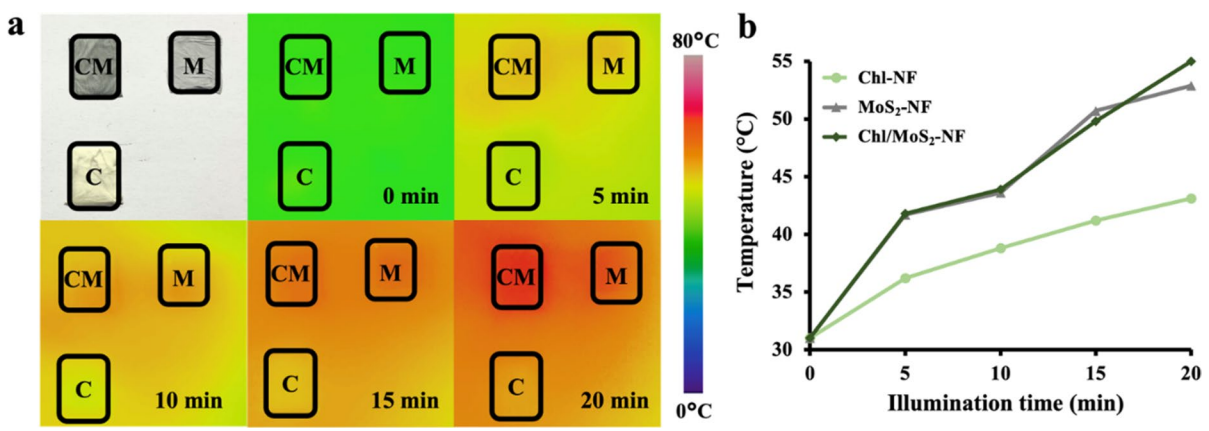

Fig. 4 Photothermal images and heating curves and of the Chl-NF (C), MoS_2-NF (M) and Chl/MoS_2-NF (CM) as a function of IR illumination time

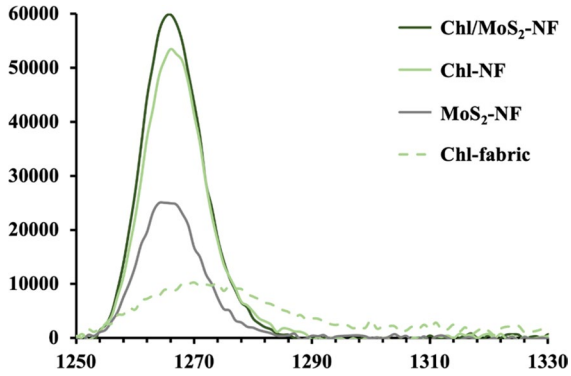

Fig. 5 Photoluminescence spectra indicative of singlet oxygen production (1270 nm Jiang et al. 2019; Mathai et al. 2007)) obtained from the visible light excitation (400 nm) of Chl-fabric, Chl-NF, MoS_2-NF and Chl/MoS_2-NF materials

chlorophyllin did not negatively affect the photothermal properties of the composite nanomaterials.

Singlet oxygen production by Chl-fabric, Chl-NF, MoS_2-NF and Chl/MoS_2-NF materials

The formation of singlet oxygen by Chl-fabric, Chl-NF, MoS_2-NF and Chl/MoS_2-NF materials under aerobic conditions and visible light illumination (400 nm) was probed using the characteristic $^1O_2$ photoluminescence peak at 1270 nm (Mathai et al. 2007). As shown in Fig. 5, both Chl-fabric and Chl-NF exhibited a photoluminescence peak consistent with singlet oxygen production. As expected, due to its higher photosensitizer loading, the signal from Chl-NF was significantly stronger than that from Chl-fabric. The $^1O_2$ photoluminescence presented by MoS_2-NF also confirmed the production of singlet oxygen by MoS_2 under illumination, and is consistent with the observation that MoS_2 can be used as both a photodynamic and a photothermal photosensitizer (Shen et al. 2021). Chl/MoS_2-NF possessed the strongest signal among all the nanofiber materials, which is attributed to the presence of both chlorophyllin and MoS_2 photosensitizers in the composite nanomaterial. Although these data cannot rule out other reactive oxygen species produced via a Type I photodynamic mechanism, the observation of singlet oxygen formation upon visible light illumination demonstrates the potential for both Chl-fabric and Chl-NF materials to at least inactivate microorganisms via a Type II mechanism. The consequence of the greater singlet oxygen production of Chl-NF on antimicrobial efficacy versus Chl-fabric will be discussed below.

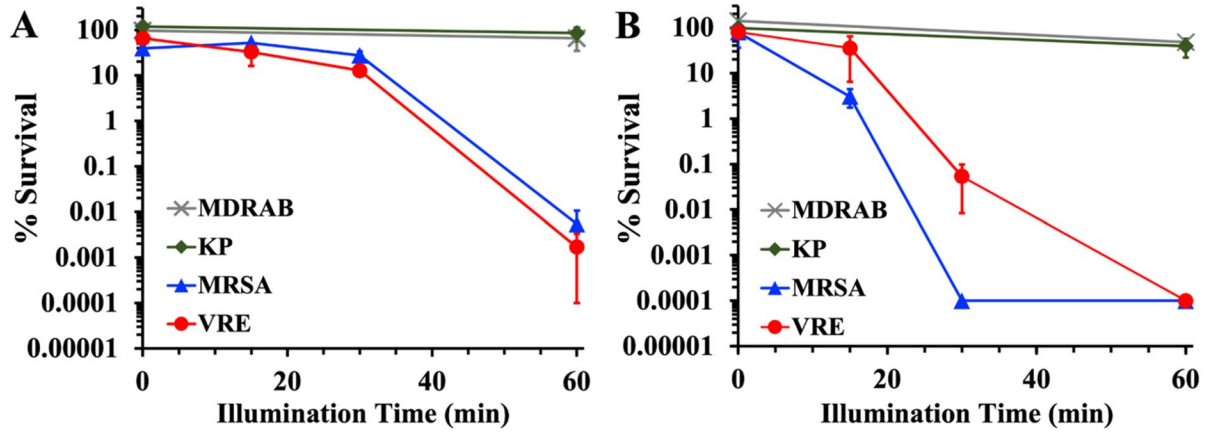

Fig. 6 Time-dependent photodynamic inactivation studies of **A** Chl-fabric and **B** Chl-NF against methicillin-resistant *S. aureus* ATCC-44 (MRSA), vancomycin-resistant *Enterococcus faecium* ATCC-2320 (VRE), multidrug-resistant *A. baumannii* ATCC-1605 (MDRAB), and NDM-1 positive *K. pneumoniae* ATCC-2146 (KP). The % survival of the dark controls after 60 min incubation are displayed as the % survival representing illumination at 0 min. For both panels, displayed are the % survival of the illuminated studies (15–60 min, 400–700 nm, 80 ± 5 mW/cm^2) compared to the material-free dark control (set as 100%)

Photodynamic antimicrobial inactivation studies

Photodynamic inactivation of Gram-positive and Gram-negative bacteria by Chl-fabric and Chl-NF

To evaluate the photodynamic antibacterial efficacy of Chl-fabric and Chl-NF in vitro, Gram-negative [multi-drug resistant *A. baumannii* ATCC-1605 (MDRAB) and *K. pneumoniae* ATCC-2146 (KP)] and Gram-positive [vancomycin-resistant *E. faecium* ATCC-2320 (VRE) and methicillin-resistant *S. aureus* ATCC-44 (MRSA)] bacteria were employed, all of which were drug-resistant. Unless otherwise noted, assays were carried out under fixed illumination conditions (400–700 nm, 80 ± 5 mW/cm^2) from 0 to 60 min and employed a starting concentration of $1–4 \times 10^8$ CFU/mL as determined by colony counting. The survival rates and *P* values were calculated based on the bacterial survival of the material-free dark controls (set as 100%). No notable inactivation was observed for any of the dark controls against MDRAB, KP, VRE and MRSA after 60 min incubation with 0 min illumination (Fig. 6). Both MDRAB and KP were found to be highly tolerant to inactivation by either Chl-fabric or Chl-NF, with < 1 log unit inactivation after 60 min illumination for both materials. This was not entirely unexpected, as it is widely accepted that, due to their more complicated cell wall structure (Malik et al. 1988), the photodynamic inactivation of Gram-negative bacteria is more difficult than for Gram positive ones. Moreover, it is known that the anionic chlorophyllin photosensitizer is generally ineffective against Gram-negative bacteria. Gratifyingly, however, both Gram-positive bacteria were found to be highly susceptible to photodynamic inactivation by Chl-fabric and Chl-NF. In the presence of Chl-fabric, both VRE and MRSA were similarly inactivated by 99.998% (4.76 log units, $P = 0.0013$) and 99.994% (4.26 log units, $P < 0.0001$), respectively, after 60 min visible light illumination. Compared to Chl-fabric, Chl-NF presented a higher inactivation efficacy against MRSA and VRE, with 99.9999% (detection limit, 6 log units, $P < 0.0001$) and 99.94% (3.27 log units, $P < 0.0001$) inactivation, respectively, after just 30 min of visible light illumination, with detection limit inactivation (99.9999%) of both pathogens after 60 min illumination (6 log units, $P = 0.0006$ for MRSA and $P = 0.0006$ for VRE). The relatively higher antibacterial efficacy of Chl-NF corresponds to its higher chlorophyllin loading compared to Chl-fabric, and is consistent with its greater singlet oxygen/ROS production noted above.

Photodynamic inactivation under low intensity illumination

To explore material performance under alternative illumination conditions, the above aPDI studies employing Chl-fabric and Chl-NF against VRE and

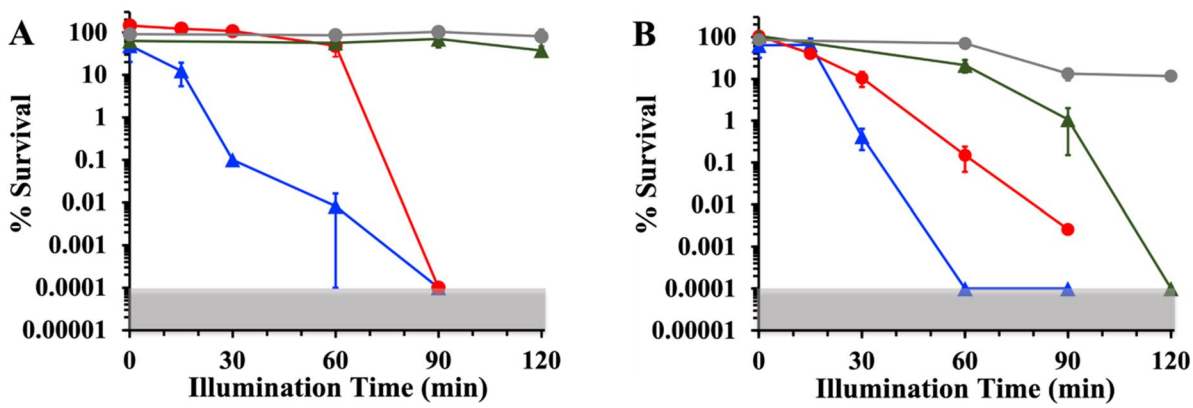

Fig. 7 Time-dependent photodynamic inactivation studies under LumaCare PDT light (400–700 nm, 30 ± 5 mW/cm^2; MRSA: blue triangle, VRE: red circle) or LED light (white light, 3 ± 1 mW/cm^2, MRSA: green triangle, VRE: grey circle) for **A** Chl-fabric and **B** Chl-NF. The % survival of the dark controls after 90 min of incubation (LumaCare PDT light) or 120 min incubation (LED light) controls are displayed as the % survival representing illumination at 0 min. For both panels, displayed are the % survival of the illuminated studies against the material-free dark controls (set as 100%)

MRSA were repeated at two lower intensity light conditions using: (1) the same LumaCare PDT light as above but at 30 ± 5 mW/cm^2 (400–700 nm), and (2) a commercially available 10 W LED white light at 3 ± 1 mW/cm^2 (Fig. 7). In the presence of Chl-fabric (Fig. 7A), with the LED light, neither MRSA nor VRE were susceptible to photodynamic inactivation even after 120 min illumination, whereas the LumaCare PDT light at the lower light intensity still yielded detection limit (99.9999%, 6 log units) inactivation of MRSA ($P = 0.0002$) and VRE ($P = 0.0013$) after 90 min illumination. As expected, due to its higher chlorophyllin content, Chl-NF exhibited better inactivation metrics (Fig. 7B): with the LED light, VRE and MRSA were inactivated by 88.4% (0.94 log units, $P < 0.0001$) and 99.9999% (detection limit, 6 log units, $P < 0.0001$), respectively, after 120 min illumination. With the LumaCare PDT light at the lower light intensity, Chl-NF was able to inactivate VRE and MRSA by 99.997% (4.58 log units, $P = 0.0003$) and 99.9999% (detection limit, 6 log units, $P < 0.0001$), respectively. Overall, both Chl-fabric and Chl-NF demonstrated the capability to inactivate both Gram-positive bacteria under lower intensity light conditions, with the Chl-NF material in particular exhibiting more promising efficacy.

Photostability of Chl-fabrics against Gram-positive S. aureus

The photostability of the Chl-fabric was assessed through both colorimetry (*K/S* value) and antibacterial photodynamic inactivation studies (Fig. 8). The *K/S* curves of Chl-fabric were recorded after 2 h illumination intervals (Xe lamp, 500 W, 15 cm sample distance, $\lambda \geq 420$ nm), and the *K/S* value at 410 nm (the characteristic absorption peak of chlorophyllin) as a function of illumination time ('photo-aged' materials) shows a gradual bleaching of the photosensitizer (Fig. 8A). Interestingly, the chlorophyllin photobleaching was only observed over the first 4 h, with the *K/S* value remaining constant afterwards. The four 'photo-aged' Chl-fabric samples (2, 4, 6, and 8 h illuminated) were employed in aPDI studies against *S. aureus* ATCC-6538, and compared to pristine Chl-fabric (0 h). The aPDI studies were carried out under fixed illumination conditions (Xe lamp, 500 W, 15 cm sample distance, $\lambda \geq 420$ nm, 60 min) and employed a starting concentration of $1–4 \times 10^8$ CFU/mL as determined by colony counting. Consistent with the decrease observed in *K/S* value upon chlorophyllin photobleaching, a decrease in inactivation efficacy from 99.96% (3.35 log units $P = 0.0026$) for pristine Chl-fabric (0 h) to 98.8% (1.95 log units, $P = 0.0078$) for 2 h 'photo-aged' Chl-fabric was observed (Fig. 8B). A more significant drop in antimicrobial

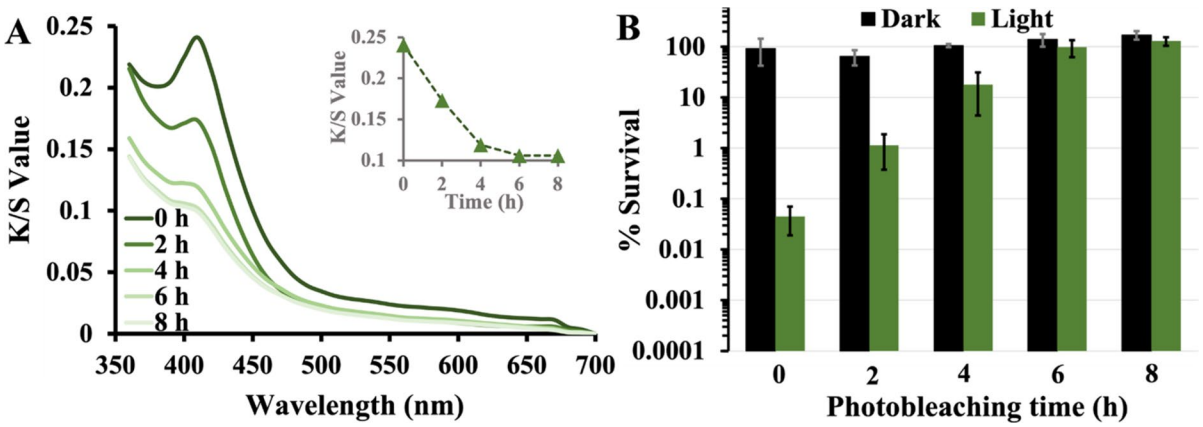

Fig. 8 **A** Illumination time dependent *K/S* curves for Chl-fabric (Xe lamp, 500 W, 15 cm sample distance, $\lambda \geq 420$ nm) for 0–8 h, inset: corresponding *K/S* values at 410 nm as a function of illumination time. **B** aPDI studies employing pristine and 'photo-aged' Chl-fabric against *S. aureus* ATCC-6538. Displayed are the % survival (*vs* material-free dark control) for the 60-min dark control (black) and illuminated (green) conditions. Illumination conditions: Xe lamp, 500 W, 15 cm sample distance, $\lambda \geq 420$ nm, 60 min

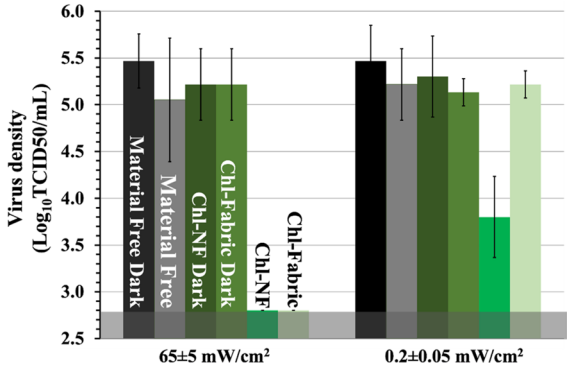

Fig. 9 Antiviral photodynamic inactivation studies employing Chl-fabric and Chl-NF against feline calicivirus (FCV). For each grouping, displayed are the material-free dark control and the material-free illuminated control (left two columns in the groups), material-present dark controls (middle columns), and the illuminated samples (right columns)

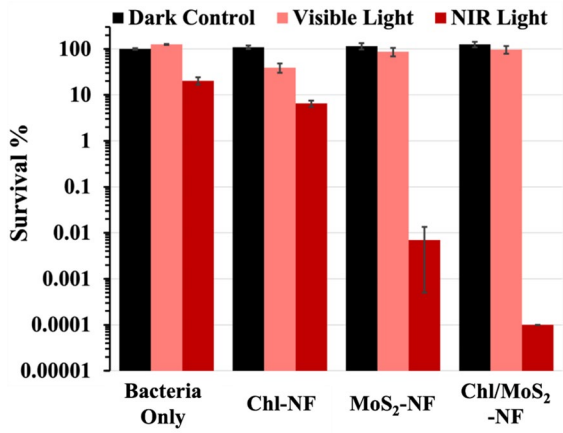

Fig. 10 Photodynamic inactivation studies of Chl-NF, MoS_2-NF, and the composite Chl/MoS_2-NF against NDM-1 positive *K. pneumoniae* ATCC-2146 (KP) under visible light (60 min, 400–700 nm, 80 ± 5 mW/cm^2) and near-infrared light (60 min, 400–825 nm, 80 ± 5 mW/cm^2) illumination. Displayed are the % survival of the dark controls with 60 min incubation (black columns), and the % survival of the illuminated studies and dark controls were calculated against the material-free dark controls (set as 100%)

efficacy was noted for the 4–8 h 'photo-aged' Chl-fabric samples. Given the high intensity of the Xe lamp used in these photo-aging studies, the results here demonstrate that Chl-fabric has the potential to be used as disposable or other short-term use textiles in hospitals and healthcare settings. Although these studies were not performed on Chl-NF, we surmise that the higher photosensitizer loading would likely translate to even better results than those shown here for Chl-fiber. Note that previous studies (Shen et al. 2021) demonstrated that MoS_2 has good photothermal stability over the short-term (≤ 6 h) intended use applications and antimicrobial studies performed here.

Photodynamic antiviral inactivation of non-enveloped FCV

The antiviral photodynamic activity of Chl-fabric and Chl-NF under either LumaCare PDT light (60 min, 65 ± 5 mW/cm^2) or common fume hood light (120 min, 0.2 ± 0.05 mW/cm^2) were evaluated against non-enveloped feline calicivirus (FCV). No considerable inactivation was observed for the material-free controls (with and without illumination, left two columns in each grouping in Fig. 9), nor for the material-present dark controls (middle two columns in the groups). In the presence of the Chl-fabric, upon LumaCare PDT light illumination, 99.8% (~2.67 log units, $P = 0.0756$) of virus (relative to the material-free dark control) was inactivated, while no statistically significant inactivation of FCV was observed upon hood light illumination (50.4% inactivation, $P = 0.2695$). Chl-NF also achieved detection limit inactivation of 2.67 log units (99.8%, $P = 0.0756$) under LumaCare PDT light illumination, and a notable inactivation of 97.6% (~1.67 log units, $P = 0.0755$) under hood light illumination. Overall, both Chl-fabric and Chl-NF demonstrated the capability to photodynamically inactivate the non-enveloped FCV virus under the relatively high light dose provided by the LumaCare PDT light, with Chl-NF still exhibiting notable photodynamic inactivation against FCV under the relatively low light dose provided by the fume hood light.

Synergistic photothermal and photodynamic antimicrobial activity of Chl/MoS_2-NF

NDM-1 positive *K. pneumoniae* ATCC-2146 (KP), the bacterium that presented < 1 log unit inactivation with Chl-NF under visible light (400–700 nm, 80 ± 5 mW/cm^2) illumination (Fig. 6), was employed to explore the synergistic antibacterial effect of the dual-agent chlorophyllin/MoS_2 composite nanofiber (Chl/MoS_2-NF). Considering the absorption of MoS_2

in the near infrared window (Shen et al. 2021), aPDI studies employing near-IR light (400–825 nm, 80 ± 5 mW/cm^2) were also performed (Fig. 10). To rule out the possibility that any observed inactivation was due to a temperature increase by NIR illumination, the % survival of the material-free (bacteria only) control under illumination is also displayed. No notable inactivation of KP was observed for any of the dark or the visible light controls. Under 60 min NIR illumination, the material-free control showed that KP was inactivated by 79% (0.69 log units, $P = 0.0004$). Given that KP is a heat-sensitive bacterium, we surmise that the temperature increase created by the NIR illumination itself is responsible for this modest level of inactivation (Mason and Hamer 1987; Verrips et al. 1979). A similar level of inactivation (~ 1 log unit) with the Chl-NF was also observed under both NIR and visible light illumination, again likely attributed to a modest rise in temperature upon illumination. Notably, however, aPDI studies with MoS_2-nanofiber showed an impressive 99.993% inactivation (4.15 log units, $P = 0.0004$) after 60 min NIR illumination. No inactivation of KP was observed with MoS_2-nanofiber under visible light illumination, consistent with MoS_2 being a NIR photothermal agent (as opposed to a photodynamic one). Impressively, the dual-agent Chl/MoS_2-NF composite nanofiber achieved detection limit inactivation of 6 log units (99.9999%, $P = 0.0004$) under NIR illumination (400–825 nm), which suggests that both MoS_2 and chlorophyllin are synergistically inactivating KP through photothermal and photodynamic mechanisms, respectively. Specifically, the 1.85 + log units greater inactivation achieved by the composite Chl/MoS_2-NF when compared to pure MoS_2-nanofiber can be ascribed to the singlet oxygen produced by chlorophyllin, despite the Chl-NF only inactivating KP by ~ 1 log unit under IR illumination (less than 1 log unit). We surmise that the singlet oxygen formed by chlorophyllin has a greater effect on the heat-stressed KP than at room temperature. Note that the temperature increase of Chl-NF is relatively minor (to 30 °C) after 20 min NIR illumination, whereas the temperature of both MoS_2-NF and the composite Chl/MoS_2-NF increased to over 50 °C under the same NIR illumination conditions (Fig. 4). The results here show that simultaneous photodynamic (chlorophyllin) and photothermal (MoS_2) inactivation mechanisms are able to synergistically yield detection limit inactivation of KP.

Conclusions

Chlorophyllin was successfully incorporated as a photosensitizer into photodynamic antimicrobial materials by both triazine coupling and electrospinning. The presence of chlorophyllin in both materials was confirmed qualitatively by visual appearance, and quantitatively by colorimetric characterization and ICP-OES elemental analysis. The addition of chlorophyllin posed no notable effects on the surfaces, morphologies or thermal stabilities of the cotton fabric or PAN nanofibers. The production of biocidal singlet oxygen by Chl-fabric and Chl-NF upon visible light illumination were confirmed by photoluminescence spectroscopy. The drug-resistant Gram-positive bacteria MRSA and VRE, and the non-enveloped FCV virus, all exhibited high susceptibility to both materials. The higher photosensitizer loading in Chl-NF led it exhibit a greater photodynamic inactivation activity than Chl-fabric. Although photobleaching at longer illumination times and high light intensities remains a challenge to overcome, the Chl-fabric presented with sufficient photostability as to be useful for disposable and other short term use textiles. While no significant inactivation of MDRAB and KP was observed owing to the known inability of chlorophyllin to inactivate Gram-negative bacteria, incorporation of the photothermal agent MoS_2 yielded a composite Chl/MoS_2-NF material capable of the detection limit inactivation (99.9999%) of KP under NIR illumination through a synergistic photothermal/photodynamic effect. While Chl/MoS_2-NF was the optimal material composition with regards to singlet oxygen yield and antibacterial efficacy against both bacterial strains examined, when considering the cost of the material relative to its corresponding antibacterial efficacy, Chl-NF is likely the better material for scalable manufacturing. Taken together, these findings suggested that the natural food colorant chlorophyllin can be grafted or embedded in the production of photodynamic antimicrobial materials for use as self-disinfecting textiles against drug-resistant Gram-positive bacteria, and that its efficacy as a photosensitizer can be synergistically amplified in the presence of a photothermal agent for use against Gram-negative pathogens.

Acknowledgments This work was supported by Suzhou Basic Research Project (SJC2023003). Part of this study was performed in the North Carolina State University Analytical

Instrumentation Facility (AIF), which is supported by the State of North Carolina and the National Science Foundation (ECCS-1542015). The AIF is a member of the North Carolina Research Triangle Nanotechnology Network (RTNN), a site in the National Nanotechnology Coordinated Infrastructure (NNCI).

Authors' contributions CJ, FS, QW, QW, and RG conceived the study and were responsible for experimental design. CJ undertook the synthesis and characterization of the materials. CJ and FJ performed the antibacterial studies. FS performed the antiviral studies. CJ wrote the main manuscript, and all authors reviewed the manuscript.

Funding This work was supported by the U.S. National Science Foundation (CNS-1844766 and IIP-2014753), as well as General Project of Jiangsu Universities Natural Science Research (No. 1020231361), Pre-research Project for NSFC of SZCU (2023SGY018), Jiangxi Provincial Natural Science Foundation (No. 20212BAB214016), Provincial Key Project of Science and Technology Innovation (No. 2022G02028), Fujian Provincial Central Guiding Local Science and Technology Development Fund Project (No. 2022L3061), Jiangsu Science and Technology Plan Special Fund (Innovation Support Plan International Science and Technology Cooperation/Hong Kong, Macao and Taiwan Science and Technology cooperation) (NO. BZ2023001), Shanghai Cooperation Organization Science and Technology Partnership Program and International Science and Technology Cooperation Program of Xinjiang Autonomous Region (No. 2022E01018).

Data availability All data are readily available upon request.

Declarations

Conflict of interest The authors have no relevant financial or non-financial interests to disclose.

Ethical approval and consent to participate Not applicable.

Consent for publication All authors reviewed the manuscript and consent to its publication.

References

Abrahamse H, Hamblin MR (2016) New photosensitizers for photodynamic therapy. Biochem J 473:347–364

Alexandrino FJR, Bezerra EM, Da Costa RF, Cavalcante LRL, Sales FAM, Francisco TS, Rodrigues LKA, de Brito DHA, Ricardo NMPS, Costa SN, de Lima-Neto P, Barroso-Neto IL, Caetano EWS, Freire VN (2019) Rose Bengal incorporated to α-cyclodextrin microparticles for photodynamic therapy against the cariogenic microorganism Streptococcus mutans. Photodiagn Photodyn Ther 25:111–118

Alvarado DR, Argyropoulos DS, Scholle F, Peddinti BST, Ghiladi RA (2019) A facile strategy for photoactive nanocellulose-based antimicrobial materials. Green Chem 21:3424–3435

Anaya-Plaza E, van de Winckel E, Mikkilä J, Malho JM, Ikkala O, Gulías O, Bresolí-Obach R, Agut M, Nonell S, Torres T, Kostiainen MA, de la Escosura A (2017) Photoantimicrobial biohybrids by supramolecular immobilization of cationic phthalocyanines onto cellulose nanocrystals. Chem Eur J 23:4320–4326

Bober P, Liu J, Mikkonen KS, Ihalainen P, Pesonen M, Plumed-Ferrer C, von Wright A, Lindfors T, Xu C, Latonen RM (2014) Biocomposites of nanofibrillated cellulose, polypyrrole, and silver nanoparticles with electroconductive and antimicrobial properties. Biomacromol 15:3655–3663

Caires CSA, Silva CM, Lima AR, Alves LM, Lima THN, Rodrigues ACS, Chang MR, Oliveira SL, Whitby C, Nascimento VA, Caires ARL (2020) Photodynamic inactivation of methicillin-resistant *staphylococcus aureus* by a natural food colorant (E-141ii). Molecules 25:4464–4475

Carpenter BL, Scholle F, Sadeghifar H, Francis AJ, Boltersdorf J, Weare WW, Argyropoulos DS, Maggard PA, Ghiladi RA (2015) Synthesis, characterization, and antimicrobial efficacy of photomicrobicidal cellulose paper. Biomacromol 16:2482–2492

Chin AWH, Chu JTS, Perera MRA, Hui KPY, Yen H-L, Chan MCW, Peiris M, Poon LLM (2020) Stability of SARS-CoV-2 in different environmental conditions. Lancet Microbe 1:e10

Decraene V, Pratten J, Wilson M (2006) Cellulose acetate containing toluidine blue and rose bengal is an effective antimicrobial coating when exposed to white light. Appl Environ Microbiol 72:4436–4439

Fadavi F, Abdulkhani A, Hamzeh Y, Bacher M, Gorfer M, Bandian D, Rosenau T, Hettegger H (2019) Photodynamic antimicrobial cellulosic material through covalent linkage of protoporphyrin IX onto lyocell fibers. J Wood Chem Technol 39:57–74

Ghareeb CR, Peddinti BST, Kisthardt SC, Scholle F, Spontak RJ, Ghiladi RA (2021) Towards universal photodynamic coatings for infection control. Front Med 8:657837

Hettegger H, Gorfer M, Sortino S, Fraix A, Bandian D, Rohrer C, Harreither W, Potthast A, Rosenau T (2015) Synthesis, characterization and photo-bactericidal activity of silanized xanthene-modified bacterial cellulose membranes. Cellulose 22:3291–3304

Jiang C, Scholle F, Ghiladi RA (2019) Mn-doped Zn/S quantum dots as photosensitizers for antimicrobial photodynamic inactivation. SPIE Bios Proc 10863:108630Q

Klemm D, Heublein B, Fink HP, Bohn A (2005) Cellulose: fascinating biopolymer and sustainable raw material. Angew Chem 44:3358–3393

Maldonado-Carmona N, Ouk TS, Calvete MJF, Pereira MM, Villandier N, Leroy-Lhez S (2020) Conjugating biomaterials with photosensitizers: advances and perspectives for photodynamic antimicrobial chemotherapy. Photochem Photobiol Sci 19:445–461

Malik Z, Ladan H, Hanania J, Nitzan Y (1988) Mesosomal structures and antimicrobial activity induced by hemin oxidation or porphyrin photodynamic sensitization in *Staphylococci*. Curr Microbiol 16:321–328

Mason CA, Hamer G (1987) Survival and activity of *Klebsiella pneumoniae* at super-optimal temperatures. Bioprocess Eng 2:121–127

Mathai S, Smith TA, Ghiggino KP (2007) Singlet oxygen quantum yields of potential porphyrin-based photosensitisers for photodynamic therapy. Photochem Photobiol Sci 6:995–1002

Messiry M, Ouffy A, Issa M (2015) Microcellulose particles for surface modification to enhance moisture management properties of polyester, and polyester/cotton blend fabrics. Alex Eng J 54:127–140

Neely AN, Maley MP (2000) Survival of *enterococci* and *staphylococci* on hospital fabrics and plastic. J Clin Microbiol 38:724–726

Norman M, Bartczak P, Zdarta J, Tomala W, Żurańska B, Dobrowolska A, Piasecki A, Czaczyk K, Ehrlich H, Jesionowski T (2016) Sodium copper chlorophyllin immobilization onto hippospongia communis marine demosponge skeleton and its antibacterial activity. Int J Mol Sci 17:1564

Peddinti BST, Scholle F, Ghiladi RA, Spontak RJ (2018) Photodynamic polymers as comprehensive anti-infective materials: staying ahead of a growing global threat. ACS Appl Mater Interfaces 10:25955–25959

Peila R, Vineis C, Varesano A, Ferri A (2013) Different methods for β-cyclodextrin/triclosan complexation as antibacterial treatment of cellulose substrates. Cellulose 20:2115–2123

Pucelik B, Sułek A, Dąbrowski JM (2020) Bacteriochlorins and their metal complexes as NIR-absorbing photosensitizers: properties, mechanisms, and applications. Coord Chem Rev 416:213340

Scott RD (2009) The direct medical costs of healthcare-associated infections in U.S. hosptials and the benefits of prevention. Centers for Disease Control and Prevention

Shen H, Jiang C, Li W, Wei Q, Ghiladi RA, Wang Q (2021) Synergistic photodynamic and photothermal antibacterial activity of in situ grown bacterial cellulose/MoS_2-chitosan nanocomposite materials with visible light illumination. ACS Appl Mater Interfaces 13:31193–31205

Stanley S, Scholle F, Zhu J, Lu Y, Zhang X, Situ X, Ghiladi R (2016) Photosensitizer-embedded polyacrylonitrile nanofibers as antimicrobial non-woven textile. Nanomaterials 6:e77

Stensberg MC, Wei Q, McLamore ES, Porterfield DM, Wei A, Sepúlveda MS (2011) Toxicological studies on silver nanoparticles: challenges and opportunities in assessment, monitoring and imaging. Nanomedicine (lond) 6:879–898

Stoll KR, Scholle F, Zhu J, Zhang X, Ghiladi RA (2019) BODIPY-embedded electrospun materials in antimicrobial photodynamic inactivation. Photochem Photobiol Sci 18:1923–1932

Tumolo T, Lanfer-Marquez UM (2012) Copper chlorophyllin: a food colorant with bioactive properties? Food Res. Int 46:451–459

Van Doremalen N, Bushmaker T, Morris DH, Holbrook MG, Gamble A, Williamson BN, Tamin A, Harcourt JL, Thornburg NJ, Gerber SI, Lloyd-Smith JO, de Wit E, Munster VJ (2020) Aerosol and surface stability of SARS-CoV-2 as compared with SARS-CoV-1. New Engl J Med 382:1564–1567

Verrips CT, Glas R, Kwast RH (1979) Heat resistance of *Klebsiella pneumoniae* in media with various sucrose concentrations. Eur J App Microbiol 8:299–308

Viera I, Pérez-Gálvez A, Roca M (2019) Green natural colorants. Molecules 24:154–171

Wang T, Xu L, Shen H, Cao X, Wei Q, Ghiladi RA, Wang Q (2020) Photoinactivation of bacteria by hypocrellin-grafted bacterial cellulose. Cellulose 27:991–1007

Wu QY, Chen XN, Wan LS, Xu ZK (2012) Interactions between polyacrylonitrile and solvents: density functional theory study and two-dimensional infrared correlation analysis. J Phys Chem B 116:8321–8330

Zhang H, Oyanedel Craver V (2013) Comparison of the bacterial removal performance of silver nanoparticles and a polymer based quaternary amine functiaonalized silsesquioxane coated point-of-use ceramic water filters. J Hazard Mater 260:272–277